Neuron
Article

Differences in Gamma Frequencies across Visual Cortex Restrict Their Possible Use in Computation

Supratim Ray[1,*] and John H.R. Maunsell[1]
[1]Department of Neurobiology and Howard Hughes Medical Institute, Harvard Medical School, 220 Longwood Avenue, Boston, MA 02115, USA
*Correspondence: supratim_ray@hms.harvard.edu
DOI 10.1016/j.neuron.2010.08.004

SUMMARY

Neuronal oscillations in the gamma band (30–80 Hz) have been suggested to play a central role in feature binding or establishing channels for neural communication. For these functions, the gamma rhythm frequency must be consistent across neural assemblies encoding the features of a stimulus. Here we test the dependence of gamma frequency on stimulus contrast in V1 cortex of awake behaving macaques and show that gamma frequency increases monotonically with contrast. Changes in stimulus contrast over time leads to a reliable gamma frequency modulation on a fast timescale. Further, large stimuli whose contrast varies across space generate gamma rhythms at significantly different frequencies in simultaneously recorded neuronal assemblies separated by as little as 400 μm, making the gamma rhythm a poor candidate for binding or communication, at least in V1. Instead, our results suggest that the gamma rhythm arises from local interactions between excitation and inhibition.

INTRODUCTION

Neuronal assemblies often exhibit stimulus-induced rhythmic activity in the gamma range (30–80 Hz), which has been suggested to play a central role in feature binding (Singer, 1999; Uhlhaas et al., 2009), to form dynamic communication channels across cortical areas processing the features of the stimulus (Fries, 2009; Womelsdorf et al., 2007), or to provide a temporal framework for the firing of neurons such that information can be coded in the timing of spikes relative to the ongoing gamma cycle (Buzsáki and Chrobak, 1995; Fries et al., 2007). These hypothesized functional roles require that the oscillation frequency be consistent across neural assemblies processing the features of a stimulus. However, previous studies have shown that the frequency of the gamma rhythm depends on simple stimulus manipulations such as size (Gieselmann and Thiele, 2008), velocity (Friedman-Hill et al., 2000; Gray and Viana Di Prisco, 1997), and cross-orientation suppression (Lima et al., 2010). In these studies, the stimulus features were changed in different trials, so in spite of variations in gamma rhythm frequency across trials, it could be used for communication or coding if the gamma frequency remained consistent across neural assemblies *within* a trial. However, for most natural stimuli, some stimulus features vary over short distances and time periods. For such stimuli, it remains unclear whether the simultaneously induced gamma rhythms in different neural assemblies that process that stimulus are stable and reliable enough to support binding, communication, or coding.

Several studies have suggested that cortical excitation can influence the gamma oscillation frequency (Ito et al., 2009; Mann and Mody, 2010; Traub et al., 1996; Whittington et al., 1995). We therefore tested whether increasing the stimulus contrast, which increases the level of cortical excitation, affects the frequency of the gamma rhythm in the primary visual cortex (V1) of two awake behaving rhesus monkeys. We then tested the dynamics of the gamma rhythm by changing the stimulus contrast over time. Finally, we tested whether gamma oscillations generated in nearby neural assemblies could remain stable and consistent for coding or communication when presented with a stimulus whose contrast varied in space.

RESULTS

Recordings were made from a chronic array of 96 electrodes (Blackrock Systems) implanted in the right hemisphere of V1. The receptive fields were in the lower left visual quadrant at an eccentricity of 3°–5°. The monkeys performed an orientation change detection task (there were two versions of the task, shown in Figure S1 and explained in detail in the Experimental Procedures section), in which they had to maintain fixation within a 1° window while two achromatic odd-symmetric Gabor stimuli were synchronously flashed for 400 ms with a mean interstimulus period of 600 ms. One stimulus was centered on the receptive field of one of the recorded sites (new location for each session; Gabor SD: 0.5°, spatial frequency: 4 cycles/°, preferred orientation); the second stimulus was located at an equal eccentricity in the other hemifield. The data shown here are from trials where the monkeys attended to the stimulus *outside* the receptive field.

First, we varied the contrast of the (unattended) stimulus inside the receptive field and studied the dependence of the gamma rhythm on stimulus contrast (we call this the "contrast study," see Experimental Procedures for details). Contrasts lower than 25% produced weak or no gamma rhythm; hence the analysis was restricted to 25%, 50%, and 100% contrast.

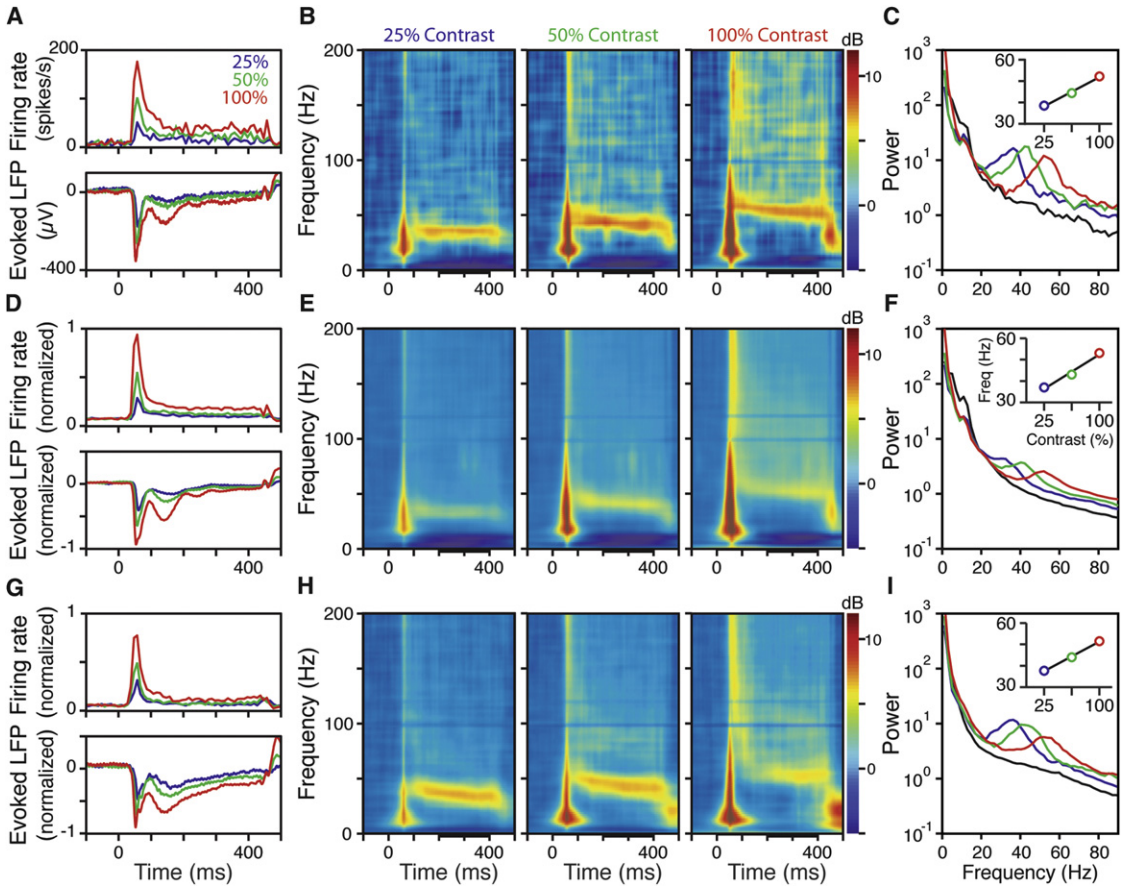

Figure 1. Gamma Rhythm Frequency Is Highly Contrast Dependent

(A) Average multiunit (upper panel) and evoked LFP response (lower panel) recorded from a single site in monkey 1 during the presentation of a static Gabor stimulus (0–400 ms), at three different contrasts: 25% (blue trace), 50% (green), and 100% (red).

(B) Time-frequency energy difference plots (in dB) showing the difference in energy from baseline energy (−300 to 0 ms, 0 denotes the stimulus onset, difference computed separately for each frequency) for the 25% (left panel), 50% (middle), and 100% (right) contrast. During the first 100 ms, there is a broadband increase in power that is associated with the sharp increase in firing rate as shown in (A). The gamma rhythm (horizontal red band) is visible only after ~100 ms, and the center frequency increases with contrast.

(C) The LFP energy between 200–400 ms (denoted by a thick black line on the x axis in B) as a function of frequency for the three contrasts. The black line shows the LFP energy in the baseline period. The inset shows the gamma frequency (the frequency between 20 and 60 Hz that has the maximum power difference from baseline) as a function of stimulus contrast. The black line in the inset shows the linear regression fit.

(D–F and G–I) Show corresponding population responses of 63 and 90 sites from monkey 1 and 2, respectively. For (D) and (G), the responses are normalized by dividing by the maximum firing rate or evoked response for each site. The SEM for the insets in (F) and (I) are smaller than the size of the symbols.

Figure 1A shows the average multiunit firing rate (upper plot) and evoked local field potential (LFP) response (lower plot) of a typical recording site from monkey 1. Figure 1B shows the change in LFP power relative to a baseline period (defined as 0–300 ms before stimulus onset) for the three contrast levels. These time-frequency energy difference spectra show a large broad-band increase in power in the first 100 ms after stimulus onset, coinciding with the transient increase in firing rate and the depolarization in the evoked LFP (Figure 1A). Although this transient increase in power occurred in a broad frequency range (from ~15 Hz to 200 Hz and beyond), including the gamma range, this should not be confused with a "rhythm." The presence of a rhythm implies an increase in power over a narrow frequency range over an extended period, which is represented by a horizontal band in a time-frequency energy difference spectrum. Such narrow-band rhythms in the gamma range appeared after ~100 ms and continued until the stimulus was turned off at 400 ms (Figure 1B). Further, the center frequency of the gamma rhythm increased with contrast. Figure 1C shows the LFP power averaged over 200–400 ms poststimulus (thick black line in Figure 1B) for the three contrasts, together with the baseline (black trace). The inset in Figure 1C shows the gamma center frequency (which was defined as the frequency between 20 and 60 Hz that showed the maximum change in power from baseline between 200 and 400 ms), as a function of stimulus contrast. Gamma frequency appeared to increase linearly with the log of contrast, and the linear fit between the center frequency and $\log_2$(contrast) had a slope of 6.8 Hz

(gamma frequency increased by 6.8 Hz when contrast was doubled). Figures 1D–1F and 1G–1I show the population average of LFP recordings from 63 and 90 sites in monkeys 1 and 2, respectively. The firing rates and evoked LFP responses were normalized by dividing by the maximum firing rate/evoked LFP response for each site before averaging (Figures 1D and 1G). The time-frequency power difference spectra (Figures 1E and 1H) and the power versus frequency spectra (Figures 1F and 1I) were averaged across sites on a log scale (see Experimental Procedures for details). The regression slopes between gamma frequency and $\log_2$(contrast) at individual sites had means of 8.0 and 6.9 for monkeys 1 and 2, both significantly greater than zero ($n = 63$, $p = 6 \times 10^{-31}$ and $n = 90$, $p = 4 \times 10^{-24}$). Overall, the center frequency moved from 37 to 53 Hz for monkey 1 and from 38 to 52 Hz for monkey 2 as contrast increased from 25% to 100%.

Because the electrode locations were fixed, the neural population recorded by an electrode may not be independent across days. The set of 63 and 90 electrodes for monkeys 1 and 2 were obtained from 23 and 59 unique electrodes, respectively (see Experimental Procedures for more details). To ensure that our results were not biased due to the presence of multiple sampling of some electrodes, we pooled the data for each unique electrode across days, computed the best frequencies as described above, and repeated the regression analysis. The regression slopes at unique electrodes had means of 8.5 and 7.3 for monkeys 1 and 2, significantly greater than zero ($n = 23$, $p = 1.8 \times 10^{-14}$ and $n = 59$, $p = 9.7 \times 10^{-19}$). For only one electrode in monkey 1 and seven electrodes in monkey 2 either the slopes were negative or less than half of the variance was explained. Thus, almost all the sites in V1 showed a strong positive correlation between contrast and gamma center frequency.

One concern is a possible interaction between stimulus-induced effects and bottom-up attention. Because stimuli of higher contrast have greater salience, they may draw more attention, which could by itself cause differences in peak gamma frequency. To address this concern, we performed the regression analysis on trials where monkey 1 attended to the stimulus inside the receptive field (this monkey performed a task in which he attended to either the stimulus outside the receptive field or inside, in different blocks of trials. See Experimental Procedures and Figure S1 for details). Whether the monkey paid attention to the stimuli inside the receptive field (the attend-in condition) or the stimuli outside the receptive field (the attend-out condition) had only a small effect on the gamma rhythm frequency. For the attend-in condition, the center frequencies at 25%, 50%, and 100% contrasts were 38.0, 44.1, and 54.5 Hz, as opposed to 37.0, 43.1, and 53.1 Hz for the attend-out condition, which were not significantly different after Bonferroni correction ($n = 63$, the uncorrected p values at 25%, 50%, and 100% contrast were 0.43, 0.22, and 0.043, t test). Similarly, the mean slope was 8.2 for the attend-in condition, as opposed to 8.0 in the attend-out condition. The two slopes were not significantly different ($n = 63$, $p = 0.77$, t test). Thus, attentional effects were weak and could not account for the large changes in gamma frequency with stimulus contrast as described above. Firing rates of the neurons also increased slightly when attention was directed inside the receptive field. Interestingly, the effect of attention on oscillation frequency was well explained by the increase in firing rate (Figure S2). This suggests a fixed relationship between firing rate and oscillation frequency that is maintained irrespective of whether firing rates vary due to contrast variations or due to shifts of attention.

Similarly, because the monkey performed an orientation change detection task, there could be memory related effects (Pesaran et al., 2002). However, that seems unlikely because gamma rhythms did not persist after the stimulus was removed (Figures 1B, 1E, and 1H). Further, the contrast of the attended stimulus outside the receptive field did not vary across presentations for monkey 2.

We next studied how LFPs and spikes were correlated between pairs of nearby electrodes and how this correlation depended on stimulus contrast. Figure 2A shows the average LFP-LFP coherence spectra at the three stimulus contrasts for 198 and 234 pairs of electrodes whose receptive fields were within 0.2° of the stimulus center, for monkeys 1 and 2 (see Experimental Procedures for details of electrode pair selection). All coherence measures were computed using the multitaper method with five tapers, with the analysis window between 150 and 406 ms after stimulus onset. Similar to the LFP power spectra shown in Figure 1, the coherence spectra showed peaks at different gamma frequencies for different contrasts. Figure 2B shows the population histogram of the relative phases between the LFPs at the peak gamma frequencies for each contrast (indicated by inverted triangles in Figure 2A). The mean phase differences were 1.0° ± 1.5°, 1.2° ± 1.8°, and 2.3° ± 1.7° (circular mean ± SE) at 25%, 50%, and 100% contrast for monkey 1 and 2.1° ± 1.9°, 1.2° ± 1.9°, and 0.4° ± 2.0° for monkey 2. These phase differences were not significantly different from zero at any contrast value ($p > 0.05$ at all contrasts for both monkeys, circular t test). Thus, gamma oscillations recorded from electrodes whose receptive fields were near the center of the stimulus were synchronous with each other.

Figure 2C shows the mean spike-LFP coherence between 185 and 155 pairs of electrodes with receptive fields within 0.2° of the stimulus center (analysis was restricted to electrodes from which at least 20 spikes were recorded in the analysis interval and for which the signal-to-noise ratio of the isolation was greater than 1.5, see Experimental Procedures for details about electrode pair selection). Again, clear peaks were observed in the gamma range, and the peak gamma frequency increased with contrast. Figure 2D shows the population histogram of the phase of the spike relative to the LFP at the peak gamma frequencies at each contrast (indicated by inverted triangles in Figure 2C). The mean phases were 140° ± 4°, 136° ± 4°, and 136° ± 3° (circular mean ± SE) at 25%, 50%, and 100% contrasts for monkey 1 and 145° ± 4°, 138° ± 3°, and 145° ± 4° for monkey 2 (shown by radial lines in Figure 2D). These phase distributions were significantly different from uniform ($p < 10^{-22}$ at all contrasts for both monkeys, Raleigh's test for nonuniformity). The mean phases at different contrasts were not significantly different from each other ($p = 0.29$ and $p = 0.71$ for monkey 1 and 2, Watson-Williams multisample test). Because the trough of the gamma cycle corresponds to 180°, these phase values implied that spikes were occurring ~40° before the gamma trough (2–3 ms, depending on the gamma frequency). This is

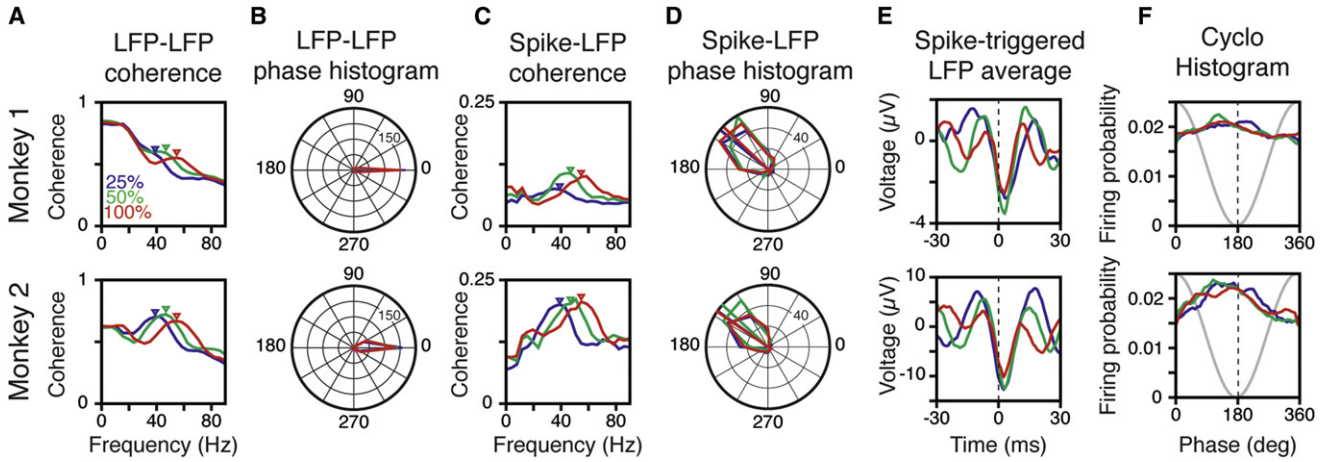

Figure 2. Relationship between Spikes and LFPs as a Function of Contrast

All analyses are shown for the interval between 150 and 406 ms poststimulus onset.

(A) The average LFP-LFP coherence between 198 and 234 pairs of electrodes for monkeys 1 and 2, whose receptive fields were within 0.2° of the stimulus center.

(B) Phase histograms of the LFP-LFP coherence values at peak gamma frequencies, indicated by inverted triangles in (A).

(C) Average spike-LFP coherence between 185 and 155 pairs of electrodes in monkeys 1 and 2, whose receptive fields were within 0.2° of the stimulus center.

(D) Phase histograms of the spike-LFP coherence values at peak gamma frequencies, indicated by inverted triangles in (C).

(E) Spike-triggered LFP average. Time of the spike (0 ms) is shown by a dotted line for clarity.

(F) Probability of a spike as a function of the phase of the gamma cycle. The gamma cycle is shown in gray. The trough of the gamma cycle (180°) is shown by a dotted line for clarity.

precisely what we observed in the spike-triggered LFP averages (Figure 2E) and the cyclohistograms, which show the firing probability of the neurons as a function of the phase of the gamma cycle (Figure 2F). Thus, spikes were influenced by the ongoing gamma oscillations, occurring preferentially 2–3 ms before the trough of the gamma cycle, and therefore showing periodicities at different frequencies at different stimulus contrasts.

To account for the multiplicity of some electrode pairs in our dataset, we repeated the analysis after first pooling data from the same pair across sessions. For the LFP-LFP analysis, out of the 198 and 234 electrode pairs described above, 105 and 210 pairs were unique. When the analysis was performed after first pooling the data for each unique pair, the mean LFP phase differences were 0.7° ± 1.7°, 1.9° ± 2.5°, and 4.1° ± 2.4° (circular mean ± SE) at 25%, 50%, and 100% contrast for monkey 1 and 1.6° ± 2.1°, 0.8° ± 2.1°, and 0.03° ± 2.2° for monkey 2, not significantly different from zero at any contrast value ($p > 0.05$ at all contrasts for both monkeys, circular t test). Similarly, for the spike-LFP analysis, out of the 185 and 155 electrode pairs, 132 and 145 pairs were unique. The mean phases were 142° ± 4°, 136° ± 4°, and 137° ± 4° (circular mean ± SE) at 25%, 50%, and 100% contrasts for monkey 1 and 144° ± 4°, 135° ± 3°, and 143° ± 4° for monkey 2. These phase distributions were significantly different from uniform ($p < 10^{-25}$ at all contrasts for both monkeys, Raleigh's test for nonuniformity). The mean phases at different contrasts were not significantly different from each other ($p = 0.64$ and $p = 0.21$ for monkey 1 and 2, Watson-Williams multisample test). All the plots for the reduced dataset closely resembled the plots shown in Figure 2 (data not shown).

Although our results show that gamma rhythms recorded at nearby electrodes near the center of the stimulus were synchronous and that spikes occurred preferentially near the trough of these gamma cycles, we failed to observe significant synchronization between pairs of spikes (Figure S3). This is consistent with previous studies that have shown that LFP-LFP and spike-LFP synchronization are typically more robust than spike-spike synchronization (Palanca and DeAngelis, 2005; Lima et al., 2010). Spike-spike coherence is much more sensitive to the precision and periodicity of spike trains than spike-LFP measures. In Figure S3, we study the effect of spike jitter and firing probability on a simulated dataset and show that in spite of significant synchronization between spikes and LFP, both the spike spectrum and autocorrelation fail to show any peaks.

Next, we asked whether rapid changes in contrast over time could modulate the gamma oscillation frequency (the "temporal frequency" study, see Experimental Procedures for details). Figure 3A shows four different contrast profiles (sinusoidal modulations at 0, 0.625, 1.25, and 2.5 Hz, with maximum contrast of 25%, 50%, and 100%). Figures 3B and 3C show the average relative change in LFP power from baseline in 44 and 90 recording sites in monkeys 1 and 2, respectively, for the 100% maximum contrast stimulus (red lines in Figure 3A). Gamma oscillation frequency showed a clear modulation when the contrast changed with time. This modulation reflected the instantaneous contrast value—gamma frequency showed a similar modulation in a lower frequency range when the maximum contrast was 50% in monkey 2 (Figure 3D). Figure 3E shows the average gamma oscillation frequency as a function of time (for each site, at each time point, the frequency between 20 and 60 Hz that had maximum power difference from baseline was chosen as the gamma oscillation frequency), for the three contrast profiles shown in Figure 3A (for monkey 1 only 25% and 100% maximum contrasts were tested). Note that the first

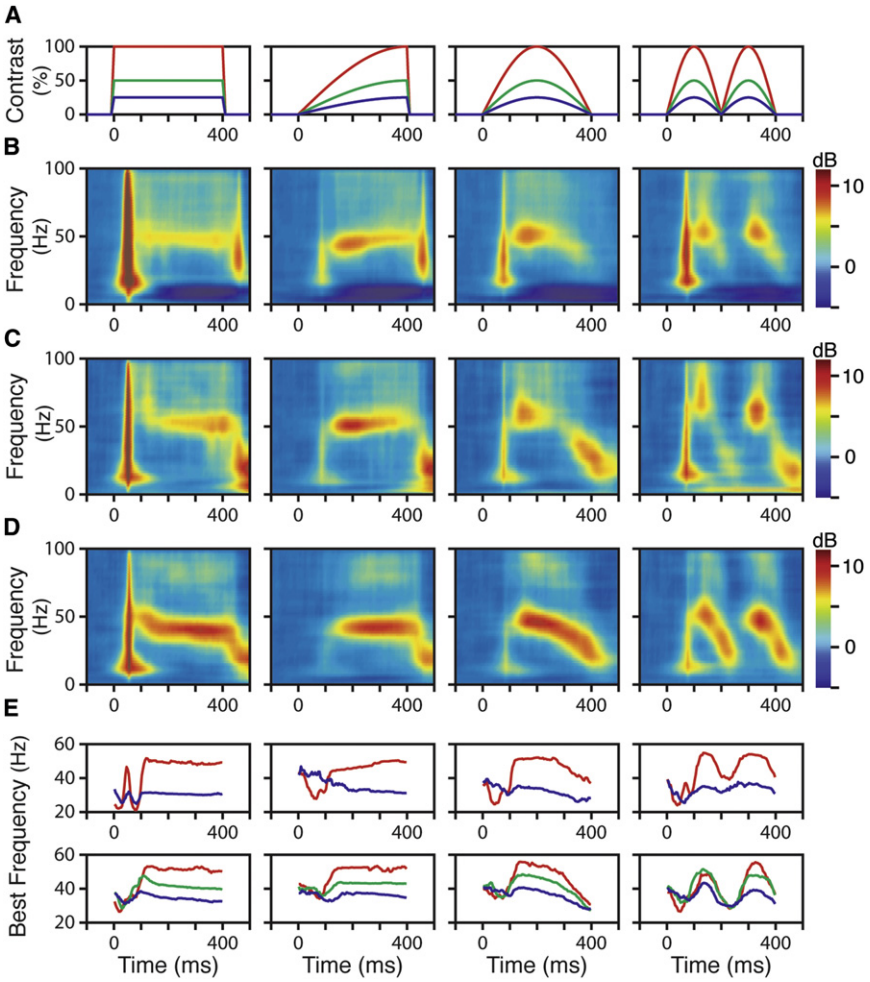

Figure 3. Changing Contrast over Time Modulates Gamma Frequency

(A) Four different contrast profiles, with temporal frequency of (from left to right) 0, 0.625, 1.25, and 2.5 Hz.

(B and C) The average time-frequency energy difference for the 100% maximum-contrast stimulus (red traces in A) for monkey 1 (44 sites, B) and monkey 2 (90 sites, C). Gamma frequency shows a pronounced modulation as the contrast changes over time.

(D) Same as (C), but for the 50% maximum-contrast stimulus (green trace in A) for monkey 2.

(E) The average gamma oscillation frequency for monkey 1 (upper panel; only 100% [red] and 25% [blue] contrasts were used for this monkey) and monkey 2 (lower panel). The standard errors were of the order of the thickness of the lines and were omitted for clarity.

100 ms after stimulus onset were dominated by sharp transients that made the estimate of gamma frequency unreliable in that period. Also note that the rise and fall of the gamma rhythm frequency were asymmetric—during the rising phase of the stimulus contrast, power of the gamma rhythm was substantial only for frequencies above ~40 Hz, but during the falling phase of the stimulus contrast gamma power was high even down to ~20 Hz (Figure 3D, third and fourth column).

Finally, we studied whether gamma oscillations are well suited for binding or communication when the stimulus contrast varies across space. Most studies that have shown significant synchronization in the gamma band have used either oriented bars or gratings (see Singer, 1999, for a review), for which the contrast is constant across space. We compared the degree of synchronization during the presentation of a grating versus a Gabor stimulus. If the gamma rhythm is important for binding or communication, the oscillation frequency and the degree of synchronization for a grating and a Gabor should be comparable. However, if the oscillation frequency only depends on the local contrast, the neural assemblies that respond to portions of the Gabor stimulus away from its center would effectively see lower contrasts, and consequently should oscillate at a lower frequency and have weak synchronization with the neurons with receptive fields near the center of the stimulus.

Figure 4A shows the receptive fields of three sites from monkey 2 that lay at varying distances from the center of a grating (left, contrast was 100% irrespective of distance from the center) and a Gabor (right) stimulus, whose contrasts was 100% at the center but decreased with increasing distance from the center. While the simultaneously recorded gamma oscillation frequencies for the grating did not change (lower left), for the Gabor stimulus they indeed decreased systematically as the distance between the stimulus center and the receptive field center increased (lower right). Figure 4B shows the average power (between 150 and 406 ms, computed using the multitaper method) for all the sites within 1° of the stimulus center, pooled into bins of size 0.2°. The data were obtained from ten recording sessions (235 and 211 electrodes for the grating and Gabor stimuli, see Experimental Procedures for details) for monkey 1 (top row) and 24 recording sessions (1383 and 1358 electrodes for the grating and Gabor stimuli) for monkey 2 (bottom row). Figure 4C shows the relationship between gamma oscillation frequency (as defined before) and the distance between stimulus and receptive field centers, for both gratings (open circles) and Gabors (filled circles). For gratings, we observed either no change (monkey 1) or a slight increase (monkey 2) in oscillation frequency, which was significant (from 47.5 at d = 0.1° to 50 Hz at d = 0.9°, $p = 4 \times 10^{-8}$, t test). This increase could be attributed to a decrease in the effective size of the stimulus for sites with receptive fields away from the stimulus center, since gamma frequency increases with decreasing stimulus size (Gieselmann and Thiele, 2008). In contrast to the gratings, we found a distinct drop in oscillation frequency for the Gabor stimulus as the distance between stimulus center and the receptive field center

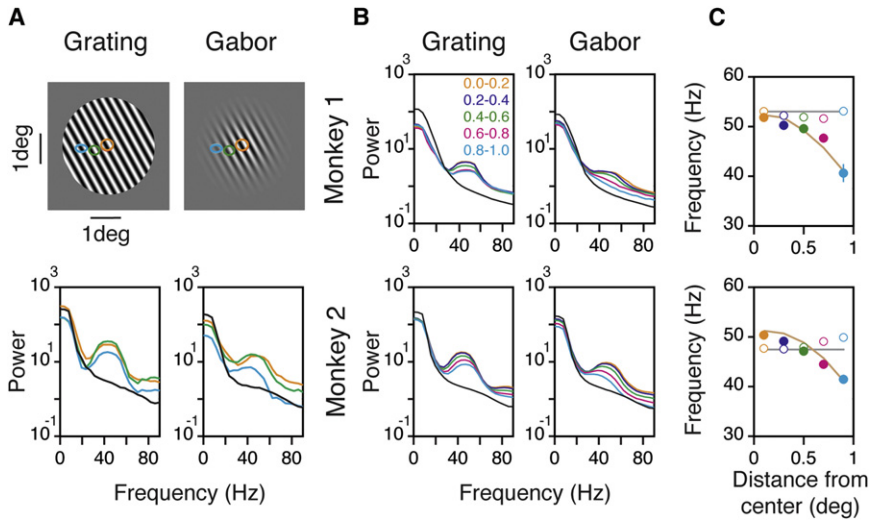

Figure 4. A Stimulus Whose Contrast Varies in Space Generates Gamma Rhythms at Different Frequencies in Different Neuronal Assemblies

(A) A grating of radius 1.56° (upper left) and a Gabor with a SD of 0.52° (upper right), both of 100% contrast at the center, along with the receptive fields of three sites at different distances from the stimulus center. The lower panels show the power spectra of the LFP (between 150 and 406 ms poststimulus onset) recorded from the three electrodes whose receptive fields are shown in the upper row. The black line shows the average LFP power during baseline. The LFPs show oscillations at different gamma frequencies depending on the distance between the receptive field center and the stimulus center for the Gabor stimulus (lower right), but not for the grating (lower left).

(B) Average population power spectra for different distances between the receptive field center and the stimulus center (binned at 0.2°), for the grating (left column) and Gabor (right column) stimulus, for monkey 1 (upper row) and monkey 2 (lower row). The five colored traces correspond to different distances, shown in the upper left panel. The black trace shows the power in the baseline period. See text for more details.

(C) Average gamma oscillation frequencies as a function of the distance between the receptive field and stimulus center for monkey 1 (upper plot) and monkey 2 (lower plot), for grating (open circles) and Gabor (closed circles) stimuli. Error bars are SEM and when not shown are smaller than the size of the symbols. The brown line indicates the estimated frequency by computing the effective contrast (the contrast within each of the receptive fields) for the Gabor stimuli and using the frequency versus contrast slopes shown in the inset of Figures 1F and 1I. The horizontal gray line shows the expected frequency for a grating stimulus, which should not vary with distance since the contrast remains constant. For monkey 2, the frequency actually increases slightly, due to a decrease in the effective size of the stimulus. See text for more details.

increased. Gamma oscillation frequency dropped by ~10 Hz for both monkeys, which was highly significant ($p < 10^{-8}$ for both monkeys, t test). We examined whether the drop in frequency could be accounted for by first computing the effective contrast within the receptive field of each neuron (estimated by reconstructing the portion of the Gabor stimulus inside the receptive field of each site and taking the difference between the maximum and minimum luminance values) and then estimating the gamma oscillation frequency from the relationship shown in the insets of Figures 1F and 1I. The estimated gamma frequencies are shown by the brown lines in Figure 4C, and they agreed well with the observed drop in frequency. Thus, a stimulus whose contrast varies in space generates gamma oscillations at significantly different frequencies in neuronal assemblies whose receptive fields are separated by as little as 0.2° (~400 μm in cortex).

This shift in oscillation frequency caused a significant reduction in synchronization among neural assemblies encoding different parts of the Gabor stimulus. Figure 5A shows the average LFP-LFP coherence between two sites, for which the receptive field of the first site was within 0.2° of the stimulus center while the other was within 1° of the stimulus center (1226 and 7778 pairs for monkeys 1 and 2, pooled into bins of size 0.2°). Figure 5B shows the values of the coherence computed at peak gamma frequency (black triangles in Figure 5A). LFP-LFP coherence values for Gabor stimuli were lower than the gratings at all distances. Further, the difference between the coherence values at peak gamma frequencies for a grating versus a Gabor stimulus (i.e., the difference between the open and closed circles in Figure 5B) increased with increasing distance between the electrodes. For example, at an electrode separation of 0.1° (orange circles in Figure 5B), the mean difference between the coherence values was 0.1 and 0.06 for monkeys 1 and 2, which increased to 0.2 and 0.11 at a distance of 0.9° (light blue circles in Figure 5B). We performed a two-way ANOVA between the coherence values with the stimulus as the first factor (two levels: grating and Gabor) and the electrode distance as the second factor (five levels: 0.1°, 0.3°, 0.5°, 0.7°, and 0.9°). Both factors were highly significant ($p < 10^{-16}$ for both the monkeys). Further, the interaction term between the two factors was also highly significant ($p = 2.1 \times 10^{-7}$ and 3.1×10^{-11} for monkeys 1 and 2). Thus, the variations in the peak gamma frequency during the presentation of the Gabor stimulus resulted in a significantly sharper decline in synchronization between neural assemblies as compared to a grating.

Figure 5C, upper row, shows the average spike-field coherence plots for 282 and 460 electrode pairs for the grating (left) and Gabor (right) stimulus for monkey 1. The lower row shows the same for 3818 and 4233 electrode pairs for monkey 2. For these electrode pairs, the "spike" electrodes had receptive field centers between 0.2° of the stimulus center, had at least 20 spikes in the analysis interval, and the signal-to-noise ratio of the isolation was greater than 1.5. The LFP electrodes had receptive fields within 1° of the stimulus center. Note that the number of pairs is smaller for gratings than Gabors, because gratings produced a much stronger suppression and thus produced lower firing rates (and fewer "spike" electrodes). A comparison between the coherence values at peak gamma frequencies (Figure 5D) showed that the spike-LFP coherence was significantly higher for the grating versus the Gabor stimulus at all electrode separations for both monkeys (two-way ANOVA returned $p < 1.5 \times 10^{-8}$ for both factors for both monkeys).

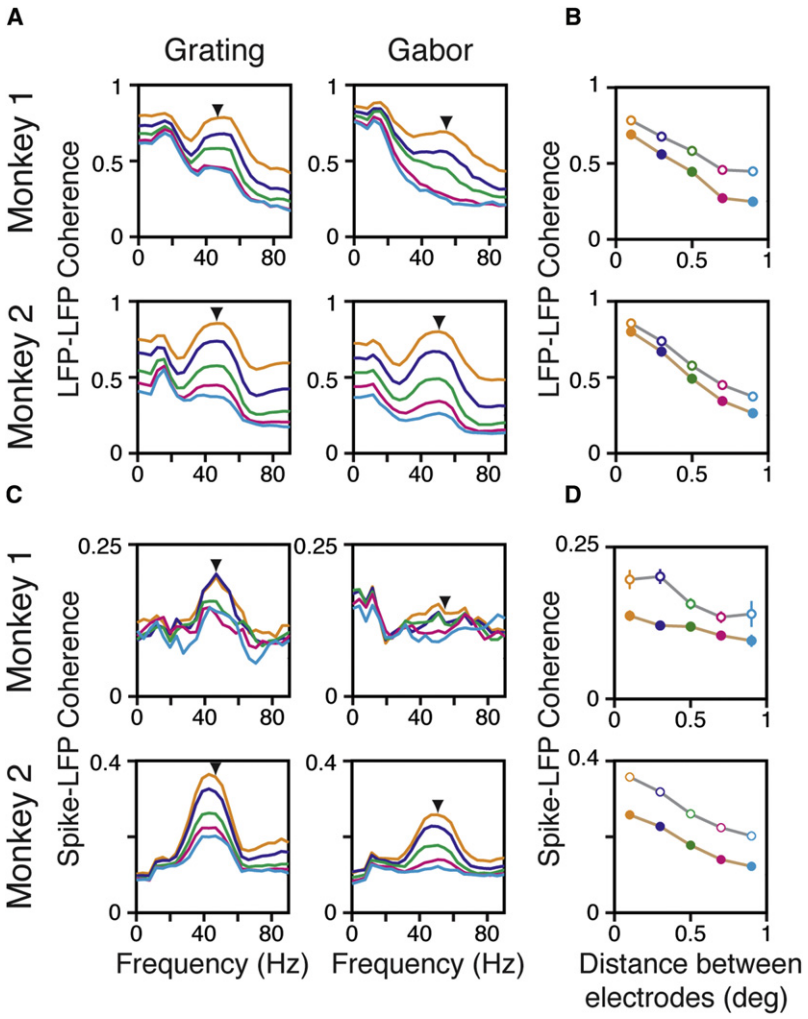

Figure 5. Comparison of LFP-LFP and Spike-LFP Coherence for Grating versus Gabor Stimuli

(A) Population LFP-LFP coherence spectra for different degree of separation between two electrodes. The five colored traces correspond to different electrode separations, shown in the upper left panel of Figure 4B. One of the electrodes in each pair is within 0.2° of the stimulus center.

(B) The average LFP-LFP coherence at the peak gamma frequency, shown by inverted triangles in (A). Coherence values for the grating and Gabor stimuli are shown with open and filled circles, respectively. The circles are connected with a gray (grating) and brown (Gabor) line for clarity.

(C and D) Same as (A) and (B), but for spike-LFP coherence. The electrode from which spikes were taken for each pair was within 0.2° of the stimulus center. See text for more details. Error bars are SEM and when not shown are smaller than the size of the symbols.

However, unlike the LFP-LFP coherence, we failed to observe a consistent increase in the difference between spike-LFP coherence values for the grating versus the Gabor stimulus with increasing electrode distance (the p values of the interaction term in the two-way ANOVA were 0.03 and 0.29 for the two monkeys). This could be attributed to several factors. First, the difference between the coherence values between the two stimuli is meaningful only when both values are much greater than the "baseline" value of ~0.1, which is obtained for a flat coherence spectrum (for example, for the Gabor stimulus at d = 0.9°, light blue traces in Figure 5C, right column). Because spike-LFP coherence values at higher electrode distances for the Gabor stimulus were close to 0.1, the effect of increasing electrode distance on the slope of spike-LFP coherence for the grating versus the Gabor was difficult to compare. Second, differences in firing rates between the two stimuli could have affected the spike-LFP measures more than the LFP-LFP measures. Third, we had fewer electrode pairs for comparison, which decreased the statistical power. To ensure that the results were not biased due to the differences in the number of electrode pairs for the grating versus the Gabor, we repeated the two-way ANOVA analysis after taking the same set of electrode pairs for the two stimuli (128 and 3285 electrode pairs for the two monkeys). The p values for the stimulus (first factor), distance (second factor), and their interaction term were (7.4×10^{-5}, 0.03, 0.26) for monkey 1 and ($<10^{-16}$, $<10^{-16}$, 0.48) for monkey 2.

For the spike-spike coherence, no peaks in the gamma range were observed for monkey 1. For monkey 2, however, we observed significant spike-spike synchronization in the gamma range, both for the grating and the Gabor stimulus. The results were very similar to the results observed from the spike-field measures and are described in Figure S4.

Although Figure 5 shows that replacing a grating with a Gabor leads to a drastic decrease in synchronization between neural assemblies encoding these stimuli, these results do not unequivocally rule out a possible role of gamma rhythms in coding or communication. For the Gabor stimulus, the "object" versus the "ground" is not as well defined as the grating, and therefore it is difficult to equate the perception of these two stimuli. Further, significant peaks in the gamma range were present in the coherence plots even for the Gabor stimulus (Figures 5A and 5C, right panels). This is because the gamma rhythm had a bandwidth of ~30 Hz, while the shift in the center frequency was only about 10 Hz. Such frequency shifts could in theory be tolerated by a neural mechanism that, for example, performs computations based on the overall power in a 30 Hz band rather than a single frequency. In the discussion section, we interpret our findings in the context of binding, communication, or coding in more detail.

DISCUSSION

We report three new results related to gamma oscillations. First, gamma oscillation frequency is highly contrast dependent. Second, temporal changes in contrast lead to corresponding

changes in gamma frequency on a fast timescale (tens to hundreds of milliseconds). Third, a stimulus whose contrast varies in space, as do most natural stimuli, causes nearby neural assemblies (~0.2° apart) to oscillate at different frequencies. The last two results suggest that gamma rhythms are generated by highly localized networks that can quickly track the incoming excitation. Further, these results suggest that the spatial spread of the LFP is less than ~400 μm, which is also supported by our observation that the receptive fields estimated from the evoked firing rates and the evoked LFP were very similar (data not shown). These results are consistent with recent studies that have estimated a spatial spread of ~250 μm for the LFP (Katzner et al., 2009; Xing et al., 2009).

A previous study by Henrie and Shapley (Henrie and Shapley, 2005) that studied the effect of contrast on gamma power did not find a systematic shift in gamma frequency with contrast. Stimuli used in that study were small (approximately the size of the receptive field) and optimized to maximize the neural response. However, the magnitude of the gamma rhythm decreases markedly for small stimuli (Gieselmann and Thiele, 2008), so the gamma rhythm generated by small stimuli may be too weak for the frequency shift to be detectable.

Matching Pursuit Algorithm for Time-Frequency Analysis

Time-frequency power spectra shown in Figures 1 and 3 were generated using the matching pursuit (MP) algorithm. MP imposes fewer a priori limitations on decomposition and has more free parameters than other methods and is able to detect local patterns in the signal with the best possible compromise between time and frequency resolution. For example, the rapid change in the spectral content of the signal with time-varying contrast that is well captured by the MP algorithm (Figure 3) is not easily revealed using traditional methods such as windowed Fourier transform. However, for the power versus frequency analysis shown in Figures 1C, 1F, and 1I, traditional methods such as short-time Fourier transform or the multitaper method gave similar results because the gamma rhythm was approximately stationary ~150 ms after stimulus onset. For example, Figures 4A and 4B show power spectra computed using the multitaper method. Similarly, the spectra obtained from matching pursuit (Figures 1C, 1F, and 1I) were compared with that obtained from the multitaper method; they were very similar (data not shown). Further details about this method and its advantages over traditional methods such as short-time Fourier transform are discussed elsewhere (Ray et al., 2008a, 2008b).

Characteristics of the Gamma Rhythm in Primary Visual Cortex of Monkeys

We describe some properties of the gamma rhythm in the primary visual cortex of monkeys before discussing their potential role in binding or coding. First, gamma rhythms are absent during periods when no stimulus is presented—no peaks in the gamma range were observed in the power spectra (black lines in Figures 1C, 1F, and 1I) or the LFP-LFP, spike-LFP and spike-spike coherence spectra (data not shown), consistent with other studies that have also failed to observe spontaneous gamma oscillations (Maldonado et al., 2000; Henrie and Shapley, 2005; Gieselmann and Thiele, 2008). Second, the first ~100 ms after stimulus onset are dominated by sharp transients in the LFP with energy in a broad frequency range, including the gamma range. The gamma rhythm becomes noticeable only ~100 ms after stimulus onset (Figures 1B, 1E, and 1H). Third, gamma rhythm is invariably weak—on average less than a few percent of the total signal power (Figures 1F and 1I); far weaker than the stimulus-evoked transient during the first 100 ms (Figures 1E, 1H, and 3B–3E). Fourth, the gamma rhythm depends critically on the stimulus properties—its power is substantially reduced if the stimulus size or spatial frequency is decreased, even though these manipulations lead to an increase in firing rate (Gieselmann and Thiele, 2008). Finally, our results show that even within a single trial, variations in stimulus properties in space and time may lead to oscillations at different gamma frequencies in nearby neural assemblies.

Considering that the latency of visual responses in V1 is ~30 ms, with the maximum rate changes between 30 and 100 ms (Figures 1A, 1D, and 1G), gamma rhythms are unlikely to play a major role in response modulation in this time period. Further, since the gamma rhythm is weak or absent under many conditions (for example, when the stimulus has low contrast, small size, null orientation, or low spatial frequency), it is unlikely to play a fundamental role in cortical processing (Fries, 2009), although specific roles under more restricted conditions cannot be ruled out. We next discuss some of the potential functional roles of gamma oscillations.

Role in Binding

In this paper, we show that the degree of synchronization depends critically on the stimulus features and decreases significantly when a stimulus has contrast that varies across space, compared to a stimulus whose contrast is constant (a Gabor versus a grating). The monkeys did not perform a task in which their perception of Gabors and gratings were quantified, so we cannot directly relate our results to the animal's perception of the different stimuli. We note, however, that most of the early studies of binding similarly did not involve any perceptual task—the animals were either anesthetized or fixating (reviewed in Singer, 1999)—and that several subsequent studies that have specifically studied a relation between gamma band synchrony and perception have failed to find conclusive evidence in support of the binding hypothesis (Lamme and Spekreijse, 1998; Thiele and Stoner, 2003; Roelfsema et al., 2004; Palanca and DeAngelis, 2005; Dong et al., 2008; Lima et al., 2010).

Gamma Phase Coding

Another suggested functional role of gamma rhythm is to set up a "clocking device" such that information could be coded in the position of the spike relative to the ongoing gamma cycle (Buzsáki and Chrobak, 1995; Fries et al., 2007). In particular, the intensity of the input could be converted to a temporal code—with stronger input leading to earlier responses in the gamma cycle (Fries et al., 2007). We found no evidence of phase coding in our dataset, for the following three reasons. First, no peaks in the gamma band could be detected for stimulus contrasts less than 25% in monkey 1 and 12.5% in monkey 2, suggesting that gamma rhythm was either absent or much

weaker than noise at low contrasts. Second, even for higher contrasts (25%–100%), there was no difference in the phase of the gamma rhythm relative to the spike (Figures 2D and 2E). Finally, the increasing oscillation center frequency of the gamma rhythm with stimulus contrast would itself confound the phase relationship, because the higher brain regions communicating with V1 would need to first decode the frequency of the gamma rhythm before any information from the phase could be obtained.

Role in Communication

Another closely related concept is that the relative phase between gamma rhythms in two cortical areas can control the degree to which they can communicate with each other—the "communication through coherence" hypothesis (Fries, 2005; Womelsdorf et al., 2007). Gamma rhythms are thought to be generated by networks of inhibitory interneurons, such that the gamma associated-IPSPs can modulate the firing probability of the pyramidal neurons (Whittington et al., 1995; Bartos et al., 2007; Cardin et al., 2009; Sohal et al., 2009). Several modeling studies have also shown that the response gain of the neurons can be changed by modulating the synchrony and phase of this rhythmic inhibition (for a review, see Tiesinga and Sejnowski, 2009).

Before we can address whether gamma rhythms can play a role in routing information between two neural assemblies, the specific details of the communication mechanism, as well as the timescale over which communication takes place must be determined. Gamma rhythms in our dataset had a bandwidth of ~30 Hz, suggesting that these rhythms were not perfectly sinusoidal, and further, showed small frequency modulations over time even when the contrast was constant (Figures 1B, 1E, 1H and Figure 3, leftmost column show that gamma center frequency decreased slightly with time). These results suggest that neural mechanisms based on these gamma rhythms must integrate power in a given frequency band instead of relying on a fixed, single frequency. Such communication channels will be more tolerant toward small shifts in operating frequencies (for example, we could observe significant synchronization for the Gabor stimulus in our dataset, as shown in the right column of Figures 5A and 5C, even though the gamma center frequencies were different). However, such channels would be less precise (for example, for two neural assemblies oscillating at gamma frequencies separated by ~10 Hz, the peak gamma frequencies would drift through all relative phases in about 100 ms). Whether such channels could be efficient and reliable enough to support neural communication remains an open question.

Another critical factor in this concept is the magnitude of the gamma rhythmic inhibition. When the magnitude of this inhibition is much greater than the intrinsic noise in the membrane potential of a neuron, it will indeed be rhythmically depolarized and hyperpolarized and its excitability will be rhythmically modulated. However, when the gamma rhythmic inhibition is weak, additional filtering mechanisms must be used to reduce the noise, which is substantial at low frequencies (because noise follows a 1/f relationship). It is unclear how such mechanisms might be incorporated by the neurons, especially when the energy of the gamma rhythm is only a few percent of the total signal energy (Figures 1F and 1I).

Gamma Rhythm as a Resonance Phenomenon

As described above, several studies have shown a role of inhibitory networks in the generation of gamma rhythms (Whittington et al., 1995; Bartos et al., 2007; Cardin et al., 2009; Sohal et al., 2009). Combined with these results, our findings support the idea that gamma rhythms are a resonant phenomenon arising from the interaction between local excitation and inhibition (Atallah and Scanziani, 2009; Brunel and Wang, 2003; Kang et al., 2009; Burns et al., 2010). Several fundamental cortical mechanisms such as divisive normalization (Heeger, 1992), adaptation (Heiss et al., 2008; Higley and Contreras, 2006), and gain control (Chance et al., 2002; Shu et al., 2003) rely on excitatory-inhibitory interactions; thus, it is not surprising that detectable gamma rhythm is also present and is modulated during a variety of cognitive tasks such as attention (Fries et al., 2001; Womelsdorf and Fries, 2007), working memory (Pesaran et al., 2002), or cortico-spinal interactions (Schoffelen et al., 2005). Thus, although our results argue against a functional role of the gamma rhythm in binding or communication in V1, it may be an important neural signature of specific types of cortical processing.

EXPERIMENTAL PROCEDURES

Behavioral Task and Recording

The animal protocols used in this study were approved by the Institutional Animal Care and Use Committee of Harvard Medical School. Recordings were made from two male rhesus monkeys (*Macaca mulatta*, 11 and 14 kg). Before training, a scleral search coil and a head post were implanted under general anesthesia. After monkeys learned the behavioral task (~4 months), we implanted a 10 × 10 array of microelectrodes (Blackrock Microsystems, 96 active electrodes) in the right primary visual cortex (about 15 mm anterior to the occipital ridge and 15 mm lateral to the midline). The microelectrodes were 1 mm long and 400 μm apart, with impedance between 0.3 and 1 MΩ at 1 kHz. The receptive fields of the neurons recorded from the microelectrodes were in the lower left quadrant of the visual space at an eccentricity of about 3°–5°.

Monkeys were trained to do two versions of an orientation-change detection task, called task 1 and task 2 (Figure S1). For both tasks, the monkey was required to hold its gaze within 1° of a small central dot (0.05°–0.10° diameter) located at the center of a CRT video display (100 Hz refresh rate, 1280 × 768 pixels, gamma corrected), while two achromatic odd-symmetric Gabor stimuli were synchronously flashed for 400 ms with a mean interstimulus period of 600 ms. One stimulus was centered on the receptive field of one of the recorded sites (new location for each session); the second stimulus was located at an equal eccentricity on the opposite side of the fixation point. In task 1, the monkey was cued to attend to one stimulus location or the other in blocks of trials. Before the start of each block, the monkey performed two instruction trials (not included in the analysis) in which there was a single stimulus. The contrasts of the attended and unattended stimuli were equal on each presentation, and could take eight possible values: 0%, 1.6%, 3.1%, 6.2%, 12.5%, 25%, 50%, and 100%, chosen pseudorandomly. In task 2, the monkey was cued to attend only to the stimulus in the right hemifield (outside the receptive field), whose contrast was fixed at a low value to make the task demanding for the monkey. Stimulus features (contrast, temporal frequency etc) at the unattended location (inside the receptive field) were varied for each stimulus presentation in a pseudorandom order.

For both tasks, at an unsignaled time drawn from an exponential distribution (mean 2000 ms, range 1000–7000 ms for monkey 1; mean 3000 ms, range 1000–7000 ms for monkey 2), the orientation of the stimulus at the

cued location changed by 90°. The monkey was rewarded with a drop of juice for making a saccade to the location of the changed stimulus within 500 ms of the orientation change. To account for saccade latency and to avoid rewarding the monkey for guessing, the monkey was rewarded only for saccades beginning at least 100 ms after the orientation change. Trials were truncated at 7000 ms if the target had not appeared (~10% of trials), in which case the animal was rewarded for maintaining fixation up to that time.

Three separate datasets were used in this study. The first set was used to study the effect of contrast (the "contrast study," Figures 1 and 2) on gamma oscillations. The second set was used to study the effect of temporal frequency (the "temporal frequency study," Figure 3). The third set was used to study how the gamma oscillation frequency varies with increasing distance between stimulus center and receptive field center (the "distance study," Figures 4 and 5).

Monkey 1 performed task 1 for the contrast study (Figures 1 and 2) in ten recording sessions. The Gabor stimuli were static with SD of 0.5°, spatial frequency of 4 cycles/°, located at the center of the receptive field of one of the sites (different recording site each session), at its preferred orientation. This monkey performed task 2 for the temporal frequency study (Figure 3) in seven recording sessions, in which the contrast of the attended stimulus (outside the receptive field) was fixed at ~3%. The stimulus inside the receptive field (unattended) was presented at two different maximum contrasts: 25% and 100% (blue and red lines in Figure 3A). For monkey 2, the contrast and temporal frequency studies were combined. This monkey performed only task 2 for 16 recording sessions, attending to a stimulus of ~7% contrast outside the receptive field while both the contrast and temporal frequency of the stimulus inside the receptive field were varied pseudorandomly. To ensure that task conditions were similar for both monkeys for the contrast study (Figures 1 and 2), we used only the trials in which monkey 1 was attending to the stimulus outside the receptive field (the attend-out condition). Typically, a larger Gabor produced a stronger gamma rhythm (Gieselmann and Thiele, 2008); hence, the effect of varying temporal frequency was also studied with a larger Gabor (SD 0.8° for monkey 1, 1° for monkey 2).

For the distance study, both monkeys performed task 2 in 10 and 24 recording sessions, attending to a Gabor of ~4.3% and ~4.5% contrast outside the receptive field, respectively. We presented static Gabor stimuli of SD 0.52°, 100% contrast, spatial frequency of 4 cycles/°, located at the center of the receptive field of one of the sites at its preferred orientation. Each session was then repeated (on different days for monkey 1, same day for monkey 2) after replacing the Gabor with a grating of radius 1.56° inside the receptive field.

Only correct trials were used for analysis. Catch trials (trials in which the orientation did not change) were excluded. For each correct trial, only the second stimulus up to the last stimulus before the target were used for analysis, so that the stimulus conditions were identical for the entire dataset. The first stimulus in each correct trial, which typically produced a stronger response, was analyzed separately, and very similar results were obtained. For monkey 1, the average number of repetitions per stimulus type was 79 for the contrast study (range 56–101) and 82 (range 31–169) for the temporal frequency study. For monkey 2, the average number of repetitions per contrast and temporal frequency was 14 (range 6–40). For the distance study, the average number of repetitions was 17 (range 8–36) for monkey 1 and 16 (range 5–28) for monkey 2.

Local field potential (LFP) and multiunits were extracted using commercial hardware and software (Blackrock System). Raw data were filtered between 0.3 and 500 Hz to extract the LFP and digitized at 2 kHz. Multiunits were extracted by filtering the raw signal between 250 and 7500 Hz followed by an amplitude threshold.

Receptive Field Mapping and Electrode Selection

Receptive fields were estimated by flashing small Gabor stimuli (SD of 0.05°–0.1°) on a 9 × 9 (monkey 1) or 11 × 11 (monkey 2) rectangular grid that spanned the receptive fields of all the electrodes, while the monkeys attended to a Gabor stimulus outside the receptive field (task 2). The evoked LFP responses and the multiunit responses at different stimulus locations were fitted separately with a 2D Gaussian to estimate the receptive field centers and sizes. Receptive fields obtained from multiunit and LFP responses were very similar. As the multiunit activity was more variable across days (and sometimes absent), we used the receptive field estimates from evoked LFP responses for analysis. For monkey 1, the upper half of the grid did not yield any responses at all. Stable estimates of the receptive field centers (SD less than 0.1° across days) were obtained from 27 electrodes in monkey 1 and 66 electrodes in monkey 2. The remaining electrodes yielded weak and inconsistent evoked responses and were excluded from analysis.

For the contrast and temporal frequency studies, for each recording session only the electrodes with receptive field centers within 0.2° of the stimulus center were used for analysis. This yielded 63 electrodes (23 unique electrodes—many electrodes were recorded on multiple sessions) for the contrast study and 44 electrodes (22 unique) for the temporal frequency study in monkey 1, and 90 electrodes (59 unique) for monkey 2.

For the LFP-LFP coherence analysis shown in Figures 2A and 2B, we took all possible pairs of sites with receptive fields within 0.2° of the stimulus center, yielding 198 pairs of electrodes for monkey 1 and 234 pairs for monkey 2. Of these, 105 and 210 pairs were unique, respectively. For the spike-LFP coherence, spike-triggered averages and cyclo-histograms (Figures 2C–2F), we first selected electrodes (with receptive fields within 0.2° of the stimulus center) from which at least 20 spikes could be recorded in the analysis interval and the signal-to-noise ratio of the isolation was greater than 1.5. This yielded 28 (16 unique) and 31 (24 unique) "spike" electrodes for monkeys 1 and 2, respectively. For each day, we took all the LFP electrodes with receptive fields within 0.2° of the stimulus center, except the spike electrode itself, yielding a total of 185 (132 unique) and 155 (145 unique) pairs of spike-LFP electrodes for monkey 1 and 2, respectively.

To account for the multiplicity of some electrodes or electrode pairs in our dataset, all statistical analyses shown in Figures 1, 2, and 3 were repeated after pooling the data from the same electrode/electrode pair across days. Very similar results were obtained.

For the distance study (Figures 4 and 5), we first took all electrodes within 1° of the stimulus center, which typically included most of the electrodes (27 for monkey 1 and 66 for monkey 2). From 10 and 24 recording sessions, we obtained 265 electrodes for monkey 1 and 1427 electrodes for monkey 2 (in this case data from an electrode cannot be pooled across sessions, because it was at a different location with respect to the stimulus center each session). Because the "best gamma frequency" was defined as the frequency between 20 to 60 Hz at which the power difference from baseline was maximum, we excluded electrodes for which the maximum power difference occurred at either 20 or 60 Hz (30 and 54 out of 265 electrodes for the grating and the Gabor stimuli for monkey 1, 44, and 69 out of 1427 for monkey 2). The analysis was also performed with the full dataset, and very similar results were obtained (data not shown).

For the LFP-LFP coherence data shown in Figures 5A and 5B, the receptive field of the first electrode was within 0.2° of the stimulus center, while the second one was at varying distances up to 1° (excluding the first electrode), yielding 1226 and 7778 pairs of LFP electrodes for monkeys 1 and 2. For the spike-LFP coherence data shown in Figures 5C and 5D, the "spike" electrode had a receptive field within 0.2° of the stimulus center, had at least 20 spikes and the signal-to-noise ratio of the isolation was greater than 1.5 (11 and 18 electrodes for the grating and Gabor stimuli for monkey 1; 65 and 72 electrodes for monkey 2). More spike electrodes were obtained for the Gabor stimulus because the grating produced a stronger suppression, leading to lower firing rates. The LFP electrode had receptive field center within 1° from the stimulus center, excluding the spike electrode. For monkey 1, we obtained 282 pairs for the grating stimulus and 460 pairs for the Gabor stimulus. For monkey 2, we obtained 3818 and 4233 pairs for gratings and Gabors, respectively. The grating versus Gabor comparison was also done after taking the same set of electrode pairs; similar results were obtained.

Data Analysis

Time-Frequency Analysis (Figures 1 and 3)

Time-frequency analysis was performed using the matching pursuit (MP) algorithm (Mallat and Zhang, 1993). MP is an iterative procedure to decompose a signal as a linear combination of members of a specified family of functions $g_{\gamma n}$, which are usually chosen to be sine-modulated Gaussians, i.e., Gabor functions or "Gabor atoms," because they give the best compromise between

frequency and time resolution. In this algorithm, a large overcomplete dictionary of Gabor atoms is first created. In the first iteration the atom $g_{\gamma 0}$ that best describes the signal $f(t)$ (i.e., has the largest inner product with it) is chosen from the dictionary and its projection onto the signal is subtracted from it. The procedure is repeated iteratively with the residual replacing the signal. Thus, during each of the subsequent iterations, the waveform $g_{\gamma n}$ is matched to the signal residue $R^n f$, which is the residue left after subtracting the results of previous iterations. Mathematical details of this method are presented elsewhere (Ray et al., 2008b). Time-frequency plots were obtained by calculating the Wigner distribution of individual atoms and taking the weighted sum (Mallat and Zhang, 1993). We have made the software used for MP computation available online at http://erl.neuro.jhmi.edu/mpsoft.

MP was performed on signals of length 4096 (−1148 ms to 900 ms at 0.5 ms resolution, where zero denotes the time of stimulus onset), yielding a 4096 × 4096 array of time-frequency energy values (with a time resolution of 0.5 ms and frequency resolution of (2000/4096) Hz = ~0.5 Hz). This was further down-sampled by a factor of 8 in the time domain and a factor of 4 in the frequency domain, yielding a time resolution of 4 ms and a frequency resolution of about 2 Hz.

Power versus frequency plots (Figures 1C, 1F, and 1I) were generated by averaging the energy within a time period at a given frequency.

$$P(\omega) = \frac{1}{T}\sum_{t=t_0}^{t_0+T} E(t,\omega) \quad (1)$$

where $E(t,\omega)$ is the mean energy averaged over trials at time t and frequency ω obtained from the MP algorithm. When showing population data (1F, 1I), we averaged the $\log_{10}(P(\omega))$ values of individual sites. The power was shown either between 200 and 400 ms (t_0 = 200, T = 200) or during baseline (t_0 = −300, T = 300).

Time-frequency difference plots (Figures 1B, 1E, 1H, 3B, 3C, and 3D) were obtained using the following equation:

$$D(t,\omega) = 10 \times (\log_{10}E(t,\omega) - \log_{10}B(\omega)) \quad (2)$$

Where $B(\omega)$ is the baseline energy as defined in Equation 1 with t_0 = −300 ms, T = 300 ms. For the population data, we averaged the $D(t,\omega)$ values of individual sites.

Coherency Analysis (Figures 2A–2D, 4, and 5)

The coherency spectrum between two signals, x and y, is defined as:

$$Coherency_{xy}(f) = \frac{S_{xy}(f)}{\sqrt{S_{xx}(f)S_{yy}(f)}} \quad (3)$$

where $S_{xy}(f)$ denotes the cross-spectrum, and $S_{xx}(f)$ and $S_{yy}(f)$ denote the auto-spectra of each signal. These were computed using the multitaper method (Thomson, 1982), implemented in Chronux 2.0 (Mitra and Bokil, 2008), an open-source, data analysis toolbox available at http://chronux.org. Essentially, the multitaper method reduces the variance of spectral estimates by pre-multiplying the data with several orthogonal tapers known as Slepian functions. Details and properties of this method can be found elsewhere (Mitra and Pesaran, 1999; Jarvis and Mitra, 2001). All data were taken between 150 and 406 ms poststimulus, at 0.5 ms resolution (512 data points). We used five tapers; the results were similar for a single or three tapers.

All circular statistics were performed using an open source circular statistics toolbox CircStat2010 (Berens and Velasco, 2009).

Regression Analysis

For characterizing the gamma frequency versus contrast relationship shown in the insets of Figures 1C, 1F, and 1I, we used the following function:

$$f = a + b\log_2(c) \quad (4)$$

where f is the gamma center frequency and c is the stimulus contrast. The parameters *a* and *b* were estimated using linear regression (Matlab, Mathworks Inc).

Behavior and Eye Positions

The behavioral task was demanding enough to require sustained attention on the stimulus. Monkey 1 was correct in 60% of the completed trials (10% missed, 30% false alarms) for the contrast study, 78% (6% missed, 16% false alarms) for the temporal frequency study, and 78% (7% missed, 15% false alarms) for the distance study. Monkey 2 was correct in 90% of the completed trials (6% missed, 4% false alarms) for the contrast and temporal frequency studies, and 92% (5% missed, 3% false alarms) for the distance study.

Eye positions were monitored at 200 Hz using a scleral search coil. The average eye positions between 200 and 400 ms across stimulus conditions differed by less than 0.03° in both monkeys and were not significantly different.

SUPPLEMENTAL INFORMATION

Supplemental Information includes four figures and can be found with this article online at doi:10.1016/j.neuron.2010.08.004.

ACKNOWLEDGMENTS

We thank Drs. Marlene Cohen, Nathan Crone, Kaushik Ghose, Mark Histed, and Ernst Niebur for helpful comments on an earlier version of the manuscript and Vivian Imamura for technical support. This work was supported by HHMI and NIH grant R01EY005911.

Accepted: July 6, 2010
Published: September 8, 2010

REFERENCES

Atallah, B.V., and Scanziani, M. (2009). Instantaneous modulation of gamma oscillation frequency by balancing excitation with inhibition. Neuron *62*, 566–577.

Bartos, M., Vida, I., and Jonas, P. (2007). Synaptic mechanisms of synchronized gamma oscillations in inhibitory interneuron networks. Nat. Rev. Neurosci. *8*, 45–56.

Berens, P., and Velasco, M.J. (2009) MPI Technical Report No. 184.

Brunel, N., and Wang, X.J. (2003). What determines the frequency of fast network oscillations with irregular neural discharges? I. Synaptic dynamics and excitation-inhibition balance. J. Neurophysiol. *90*, 415–430.

Burns, S.P., Xing, D., Shelley, M.J., and Shapley, R.M. (2010). Searching for autocoherence in the cortical network with a time-frequency analysis of the local field potential. J. Neurosci. *30*, 4033–4047.

Buzsáki, G., and Chrobak, J.J. (1995). Temporal structure in spatially organized neuronal ensembles: a role for interneuronal networks. Curr. Opin. Neurobiol. *5*, 504–510.

Cardin, J.A., Carlén, M., Meletis, K., Knoblich, U., Zhang, F., Deisseroth, K., Tsai, L.H., and Moore, C.I. (2009). Driving fast-spiking cells induces gamma rhythm and controls sensory responses. Nature *459*, 663–667.

Chance, F.S., Abbott, L.F., and Reyes, A.D. (2002). Gain modulation from background synaptic input. Neuron *35*, 773–782.

Dong, Y., Mihalas, S., Qiu, F., von der Heydt, R., and Niebur, E. (2008). Synchrony and the binding problem in macaque visual cortex. J. Vis. *8*, 1–16.

Friedman-Hill, S., Maldonado, P.E., and Gray, C.M. (2000). Dynamics of striate cortical activity in the alert macaque: I. Incidence and stimulus-dependence of gamma-band neuronal oscillations. Cereb. Cortex *10*, 1105–1116.

Fries, P. (2005). A mechanism for cognitive dynamics: neuronal communication through neuronal coherence. Trends Cogn. Sci. *9*, 474–480.

Fries, P. (2009). Neuronal gamma-band synchronization as a fundamental process in cortical computation. Annu. Rev. Neurosci. *32*, 209–224.

Fries, P., Reynolds, J.H., Rorie, A.E., and Desimone, R. (2001). Modulation of oscillatory neuronal synchronization by selective visual attention. Science *291*, 1560–1563.

Fries, P., Nikolić, D., and Singer, W. (2007). The gamma cycle. Trends Neurosci. *30*, 309–316.

Gieselmann, M.A., and Thiele, A. (2008). Comparison of spatial integration and surround suppression characteristics in spiking activity and the local field potential in macaque V1. Eur. J. Neurosci. *28*, 447–459.

Gray, C.M., and Viana Di Prisco, G. (1997). Stimulus-dependent neuronal oscillations and local synchronization in striate cortex of the alert cat. J. Neurosci. *17*, 3239–3253.

Heeger, D.J. (1992). Normalization of cell responses in cat striate cortex. Vis. Neurosci. *9*, 181–197.

Heiss, J.E., Katz, Y., Ganmor, E., and Lampl, I. (2008). Shift in the balance between excitation and inhibition during sensory adaptation of S1 neurons. J. Neurosci. *28*, 13320–13330.

Henrie, J.A., and Shapley, R. (2005). LFP power spectra in V1 cortex: the graded effect of stimulus contrast. J. Neurophysiol. *94*, 479–490.

Higley, M.J., and Contreras, D. (2006). Balanced excitation and inhibition determine spike timing during frequency adaptation. J. Neurosci. *26*, 448–457.

Ito, I., Bazhenov, M., Ong, R.C., Raman, B., and Stopfer, M. (2009). Frequency transitions in odor-evoked neural oscillations. Neuron *64*, 692–706.

Jarvis, M.R., and Mitra, P.P. (2001). Sampling properties of the spectrum and coherency of sequences of action potentials. Neural Comput. *13*, 717–749.

Kang, K., Shelley, M., Henrie, J.A., and Shapley, R. (2009). LFP spectral peaks in V1 cortex: network resonance and cortico-cortical feedback. J. Comput. Neurosci., in press. 10.1007/s10827-009-0190-2.

Katzner, S., Nauhaus, I., Benucci, A., Bonin, V., Ringach, D.L., and Carandini, M. (2009). Local origin of field potentials in visual cortex. Neuron *61*, 35–41.

Lamme, V.A.F., and Spekreijse, H. (1998). Neuronal synchrony does not represent texture segregation. Nature *396*, 362–366.

Lima, B., Singer, W., Chen, N.H., and Neuenschwander, S. (2010). Synchronization dynamics in response to plaid stimuli in monkey V1. Cereb. Cortex *20*, 1556–1573.

Maldonado, P.E., Friedman-Hill, S., and Gray, C.M. (2000). Dynamics of striate cortical activity in the alert macaque: II. Fast time scale synchronization. Cereb. Cortex *10*, 1117–1131.

Mallat, S.G., and Zhang, Z. (1993). Matching pursuits with time-frequency dictionaries. IEEE Trans. Signal Process *41*, 3397–3415.

Mann, E.O., and Mody, I. (2010). Control of hippocampal gamma oscillation frequency by tonic inhibition and excitation of interneurons. Nat. Neurosci. *13*, 205–212.

Mitra, P., and Bokil, H. (2008). Observed Brain Dynamics (New York: Oxford University Press).

Mitra, P.P., and Pesaran, B. (1999). Analysis of dynamic brain imaging data. Biophys. J. *76*, 691–708.

Palanca, B.J.A., and DeAngelis, G.C. (2005). Does neuronal synchrony underlie visual feature grouping? Neuron *46*, 333–346.

Pesaran, B., Pezaris, J.S., Sahani, M., Mitra, P.P., and Andersen, R.A. (2002). Temporal structure in neuronal activity during working memory in macaque parietal cortex. Nat. Neurosci. *5*, 805–811.

Ray, S., Crone, N.E., Niebur, E., Franaszczuk, P.J., and Hsiao, S.S. (2008a). Neural correlates of high-gamma oscillations (60-200 Hz) in macaque local field potentials and their potential implications in electrocorticography. J. Neurosci. *28*, 11526–11536.

Ray, S., Hsiao, S.S., Crone, N.E., Franaszczuk, P.J., and Niebur, E. (2008b). Effect of stimulus intensity on the spike-local field potential relationship in the secondary somatosensory cortex. J. Neurosci. *28*, 7334–7343.

Roelfsema, P.R., Lamme, V.A., and Spekreijse, H. (2004). Synchrony and covariation of firing rates in the primary visual cortex during contour grouping. Nat. Neurosci. *7*, 982–991.

Schoffelen, J.M., Oostenveld, R., and Fries, P. (2005). Neuronal coherence as a mechanism of effective corticospinal interaction. Science *308*, 111–113.

Shu, Y., Hasenstaub, A., Badoual, M., Bal, T., and McCormick, D.A. (2003). Barrages of synaptic activity control the gain and sensitivity of cortical neurons. J. Neurosci. *23*, 10388–10401.

Singer, W. (1999). Neuronal synchrony: a versatile code for the definition of relations? Neuron *24*, 49–65, 111–125.

Sohal, V.S., Zhang, F., Yizhar, O., and Deisseroth, K. (2009). Parvalbumin neurons and gamma rhythms enhance cortical circuit performance. Nature *459*, 698–702.

Thiele, A., and Stoner, G. (2003). Neuronal synchrony does not correlate with motion coherence in cortical area MT. Nature *421*, 366–370.

Thomson, D.J. (1982). Spectrum estimation and harmonic analysis. Proc. IEEE *70*, 1055–1096.

Tiesinga, P., and Sejnowski, T.J. (2009). Cortical enlightenment: are attentional gamma oscillations driven by ING or PING? Neuron *63*, 727–732.

Traub, R.D., Whittington, M.A., Colling, S.B., Buzsáki, G., and Jefferys, J.G. (1996). Analysis of gamma rhythms in the rat hippocampus in vitro and in vivo. J. Physiol. *493*, 471–484.

Uhlhaas, P.J., Pipa, G., Lima, B., Melloni, L., Neuenschwander, S., Nikolić, D., and Singer, W. (2009). Neural synchrony in cortical networks: history, concept and current status. Front. Integr. Neurosci. *3*, 17.

Whittington, M.A., Traub, R.D., and Jefferys, J.G. (1995). Synchronized oscillations in interneuron networks driven by metabotropic glutamate receptor activation. Nature *373*, 612–615.

Womelsdorf, T., and Fries, P. (2007). The role of neuronal synchronization in selective attention. Curr. Opin. Neurobiol. *17*, 154–160.

Womelsdorf, T., Schoffelen, J.M., Oostenveld, R., Singer, W., Desimone, R., Engel, A.K., and Fries, P. (2007). Modulation of neuronal interactions through neuronal synchronization. Science *316*, 1609–1612.

Xing, D., Yeh, C.I., and Shapley, R.M. (2009). Spatial spread of the local field potential and its laminar variation in visual cortex. J. Neurosci. *29*, 11540–11549.